# Behavior of Different Calcium-Based Sorbents in a Calcination/Carbonation Cycle for $CO_2$ Capture

Diego Alvarez,* Miguel Peña, and Angeles G. Borrego

*Instituto Nacional del Carbón, CSIC, P. O. Box 73, 33080 Oviedo, Spain*

*Received November 15, 2006. Revised Manuscript Received February 13, 2007*

The aim of this work is to identify the characteristics of natural carbonates which upon calcination generate an optimum material for use as a $CO_2$-capturing sorbent in large-scale industrial $CO_2$-producing sources. Nine different naturally occurring Ca/Mg carbonates were selected for this study. The carbonates were fully characterized by a variety of analytical techniques including atomic absorption and redox volumetry, for the chemical characterization of the carbonates, and optical and scanning electron microscopy (SEM), X-ray diffraction, and Fourier transform infrared spectroscopy, to determine their crystallinity, morphology, and the presence of impurities. They were then subjected to successive (up to 100) calcination/recarbonation cycles, and their conversion decay curves were interpreted on the basis of the physical and chemical characteristics of the parent carbonates. The textural development of the sorbents during cycling was studied by Hg porosimetry and SEM. Hardness tests were also conducted on selected samples. It was concluded that both carbonate purity and crystallinity are important parameters in determining the performance of the sorbents. The activity of all the sorbents tested turned out to be highly dependent on the pore structure of the calcines and their variation during cycling. In turn, the natural tendency of the sorbents to develop low surface areas (poor efficiencies) during cycling seems to be enhanced by the presence of moderate amounts of Mg.

## Introduction

The ability of CaO to reversibly react with $CO_2$ can be used as a means of capturing the carbon dioxide released from large stationary $CO_2$-emitting sources, such as power plants and cement, steel, or paper industries, which could then be safely stored in a variety of natural reservoirs, thus curbing the emissions of this greenhouse gas to the atmosphere. The cyclic carbonation/calcination reaction has been proposed as a means of capturing the $CO_2$ produced during fossil fuel combustion for electricity generation,[1−7] obtaining $CO_2$-free $H_2$,[8−11] storing energy,[12,13] or as a chemical heat pump.[13,14]

Limestones have many advantages over other $CO_2$ sorbents, among which are their low cost, wide availability, and flexibility of use under conditions which would be very hostile to methanol, amines, membranes, and so forth. Also, the exothermic $CO_2$ absorption takes place at high temperatures (above 650 °C), and thus the energy released can be more efficiently utilized than in low-temperature absorption systems. Calcined limestones can react with the $CO_2$-containing exhaust gases from virtually any industrial process, and the recarbonated sorbents obtained can be regenerated (calcined) in a separate reactor, producing a stream of pure $CO_2$ for further sequestration. The process is not without disadvantages, the most important being the continuous loss of activity that the sorbents undergo with the number of calcination/recarbonation cycles.[1,5,8,9,12,13,15] Finding a way to attenuate this activity drop is thus a key issue for the applicability of this capture method. The sorbent particles must also be physically resistant to thermal shock and abrasion,

* Corresponding author. Phone: +34 985119090. Fax: +34 985297662. E-mail: diegoalv@incar.csic.es.

(1) Shimizu, T.; Hirama, T.; Hosoda, H.; Kitano, K.; Inagaki, M.; Tejima, K. A Twin Fluid-Bed Reactor for Removal of $CO_2$ from Combustion Processes. *Trans. Inst. Chem. Eng.* **1999**, *77A*, 62−68.

(2) Gupta, H.; Fan, L. S. Carbonation−Calcination Cycle Using High Reactivity Calcium Oxide for Carbon Dioxide Separation from Flue Gas. *Ind. Eng. Chem. Res.* **2002**, *41* (16), 4035−4042.

(3) Griffin, T; Bill, A.; Marion, J. L; Nsakala, N. $CO_2$ Control Technologies. Alstom Power Approach. *Proceedings of the 6th International Conference on Greenhouse Gas Control Technologies*, Kyoto, Japan; Gale, J., Kaya, Y., Eds.; Elsevier: Amsterdam, 2003; Vol. I, p 81.

(4) Abanades, J. C.; Oakey, J. E.; Alvarez, D.; Hämäläinen, J. Novel Combustion Cycles Incorporating Capture of $CO_2$ with CaO. *Greenhouse Gas Control Technologies*; GHGT-6: Kyoto, Japan, 2003; pp 181−187.

(5) Abanades, J. C.; Alvarez, D. Conversion Limits in the Reaction of $CO_2$ with Lime. *Energy Fuels* **2003**, *17*, 308−315.

(6) Abanades, J. C.; Anthony, E. J.; Lu, D. Y.; Salvador, C.; Alvarez, D. Capture of $CO_2$ from Combustion Gases in a Fluidized Bed of CaO. *Environ. Sci. Technol.* **2004**, *50* (7), 1614−1622.

(7) Hughes, R. W.; Lu, D.; Anthony, E. J.; Wu, Y. Improved Long-Term Conversion of Limestone Derived Sorbents for in Situ Capture of $CO_2$ in a Fluidised Bed Combustor. *Ind. Eng. Chem. Res.* **2004**, *43*, 5529−5539.

(8) Curran, G. P.; Fink, C. E.; Gorin, E. Carbon Dioxide-Acceptor Gasification Process. Studies of Acceptor Properties. *Adv. Chem. Ser.* **1967**, *69*, 141.

(9) Silaban, A.; Harrison, D. P. High Temperature Capture of Carbon Dioxide: Characteristics of the Reversible Reaction Between CaO(s) and $CO_2$(g). *Chem. Eng. Commun.* **1995**, *137*, 177.

(10) Lin, S. Y.; Suzuki, Y.; Hatano, H.; Harada, M. Developing an Innovative Method, HyPr-RING, to Produce Hydrogen from Hydrocarbons. *Energy Convers. Manage.* **2002**, *43*, 9−12; 1283−1290.

(11) Bandi, A.; Specht, M.; Sichler, P.; Nicoloso, N. In Situ Gas Conditioning in Fuel Reforming for Hydrogen Generation. 5th International Symposium on Gas Cleaning at High Temperature, Morgantown, WV, Sept, 2002; NETL: Morgantown, WV, 2002; pp 17−20.

(12) Barker, R. The Reversibility of the Reaction $CaCO_3 \leftrightarrow CaO + CO_2$. *J. Appl. Chem. Biotechnol.* **1973**, *23*, 733−742.

(13) Aihara, M.; Nagai, T.; Matsushita, J.; Negishi, Y.; Ohya, H. Development of Porous Solid Reactant for Thermal-Energy Storage and Temperature Upgrade Using Carbonation/Decarbonation Reaction. *Appl. Energy* **2001**, *69*, 225−238.

(14) Kato, Y.; Yamada, M.; Kanie, T.; Yoshizawa, Y. Calcium oxide/carbon dioxide reactivity in a packed bed reactor of a chemical heat pump for high-temperature gas reactors. *Nucl. Eng. Des.* **2001**, *210*, 1−8.

(15) Deutch, Y.; Heller-Kallai, L. Decarbonation and Recarbonation of Calcites Heated in $CO_2$, Part 1, Effect of the Thermal Regime. *Thermochim. Acta* **1991**, *182*, 77−89.

10.1021/ef060573i CCC: $37.00 
Published on Web 03/30/2007

both in calcined and recarbonated forms, as the material is to be subjected to temperature swings and fluidized-bed conditions, where the attrition of the sorbent might become a major problem. The performance of a given calcareous sorbent in a calcination/carbonation loop depends on its specific behavior during calcination and, more importantly, during recarbonation.

The thermal decomposition (calcination) of calcium carbonate is one of the most widely studied chemical reactions, unlike reverse lime recarbonation, which has so far merited relatively little attention due to its limited usefulness. Even less is known about the behavior of the carbonates when subjected to repeated calcination/recarbonation cycles; although the potential of this calcium loop system for the capture of $CO_2$ from the exhaust gases of a variety of chemical processes with the aim of reducing the emission of this greenhouse gas to the atmosphere has led to a renewed interest in the study of these reactions. The course of both reactions can be briefly described as follows:

(1) Calcination takes place on a receding interface, according to a shrinking core model, and the product layer consists of a network of CaO micrograins which is highly porous (∼54%) due to the different molar volumes of carbonate and oxide (36.9 and 16.9 $cm^3\ mol^{-1}$, respectively).

(2) Recarbonation occurs on the surface of the CaO micrograins, and a carbonate layer is formed. This layer then moves toward the center of the micrograins. The reaction works very fast until the product layer reaches a thickness of about 50−100 nm. If some CaO still exists in the inner core of the micrograins, it will only react very slowly in a diffusion-controlled stage.

Despite the apparent simplicity of this scheme, the calcination reaction is extremely complex from the point of view of the quality of the lime produced. To quote Boynton[16] "...this process still remains to some extent a technique or an art that only an experienced lime burner fully comprehends". One of the main factors responsible for the scattering of results, in terms of lime morphology and reactivity, is the sintering of the newly formed CaO that takes place during the calcination of the limestone particles, driven by temperature and catalyzed by the $CO_2$ evolving from the core of the particles.[17,18] Such sintering will take place to different extents depending on the calcination conditions, mainly temperature and $CO_2$ concentration, and on the characteristics of the parent carbonate, especially its crystal size and chemical purity. The larger the crystal size, the more stresses it will undergo, leading to the formation of a network of cracks[19] which will facilitate both calcination and recarbonation through the enlargement of the reacting interface. Moreover, certain ion impurities may enhance sintering by facilitating the ionic mobility in the CaO groundmass.

When the above-mentioned scenario for lime recarbonation is assumed, care should be taken to avoid excessive sintering of the lime produced in calcination so that no unreacted cores are left in the interior of the CaO micrograins. At the same time, they should not be so small as to block the pore network due to the formation of a sealing carbonate layer in the outer part of the particles.[20] To achieve this, we must be very careful in our choice of the parent carbonate, as the operating conditions are largely conditioned by the very objective pursued in cycling the sorbent: calcination necessarily has to take place in a 100% $CO_2$ atmosphere if a stream of pure $CO_2$ is to be obtained, and the equilibrium temperature of calcination under these conditions[21] is 898 °C at 1 bar pressure, so that an extra few degrees centigrade need to be supplied in order to speed up the reaction. Even if the partial pressure of $CO_2$ is reduced, either by application of reduced pressures (mild vacuum) or by dilution with an easily removable gas such as steam, temperatures around 850 °C would still be required to calcine the carbonated sorbents under a 0.2 bar $CO_2$ partial pressure. The first solution looks complicated, from an operational point of view, and the second involves the use of large amounts of very high temperature steam, which is known to have a stronger catalytic effect on CaO sintering than the $CO_2$ itself.[22] In any case, the environmental conditions required for calcination are highly sintering, and so much care should be taken to choose an optimum sorbent, with a limited tendency to sinter.

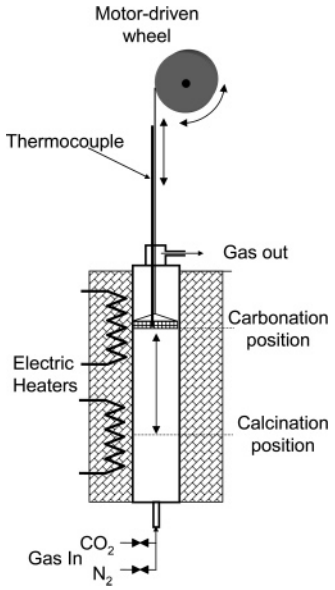


**Figure 1.** Scheme of the experimental setup used.

The most suitable design for the calciner and the recarbonator reactors is the fluidized bed, where the sorbent particles would be subjected to extensive mechanical shock, leading to the formation of fine grains which would be elutriated from the reactors. It is therefore essential that the sorbent particles are hard enough to preserve their integrity during the largest possible number of cycles. Another factor which could affect the particle size distribution of the sorbents is the thermal shock that the particles undergo when they first enter the calciner and, to a lesser extent, when they are transferred from the carbonator (∼650 °C) to the calciner (∼950 °C). Both the thermal and the mechanical strength are conditioned by the crystal arrangement of the parent sorbents.[16]

This work explores the capabilities of different naturally occurring carbonates as raw materials to act as $CO_2$ sorbents in a calcium looping system intended for $CO_2$ capture from large stationary sources such as power stations, steel or cement

(16) Boynton, R. S. *Chemistry and Technology of Lime and Limestone*; John Wiley & Sons: New York, 1980.

(17) Borgwardt, R. H. Calcination Kinetics and Surface Area of Dispersed Limestone Particles. *AIChE J.* **1985**, *31* (1), 103−111.

(18) Fuertes, A. B.; Alvarez, D.; Rubiera, F.; Pis, J. J.; Marbán G. Surface Area and Pore Size Changes during Sintering of Calcium Oxide Particles. *Chem. Eng. Commun.* **1991**, *109*, 73−88.

(19) Satterfied, C. N.; Feakes, F. *AIChE J.* Kinetics of the thermal Decomposition of Calcium Carbonate. **1959**, *5*,115−122.

(20) Alvarez, D.; Abanades, J. C. Pore-Size and Shape Effects on the Recarbonation Performance of Calcium Oxide Submitted to Repeated Calcination/Recarbonation Cycles. *Energy Fuels* **2005**, *19*, 270−278.

(21) Baker, E. H. The Calcium Oxide-Carbon Dioxide System in the Pressure Range 1−300 Atmospheres. *J. Chem. Soc.* **1962**, *87*, 464−470.

(22) Borgwardt R. H. Calcium Oxide Sintering in Atmospheres Containing Water and Carbon Dioxide. *Ind. Eng. Chem. Res.* **1989**, *28*, 493−500.

**Table 1. Chemical Characterization of Samples**

| | wt.% | | | | | | | | |
|---|---|---|---|---|---|---|---|---|---|
| | CaO | MgO | SrO | $Na_2O$ | $K_2O$ | $SiO_2$ | $Fe_2O_3$ | $Al_2O_3$ | LOC[a] |
| B | 55.67 | 0.15 | 0.02 | 0.03 | 0.04 | 0.00 | 0.00 | 0.00 | 43.96 |
| H | 54.90 | 0.33 | 0.09 | 0.03 | 0.07 | 0.51 | 0.11 | 0.25 | 43.34 |
| C | 51.97 | 2.55 | 0.12 | 0.19 | 0.20 | 0.79 | 0.14 | 0.42 | 44.61 |
| P | 54.32 | 0.61 | 0.07 | 0.05 | 0.04 | 0.51 | 0.53 | 0.21 | 42.64 |
| K | 53.83 | 1.11 | 0.05 | 0.04 | 0.05 | 0.00 | 0.11 | 0.19 | 42.39 |
| M | 55.58 | 0.88 | 0.05 | 0.03 | 0.05 | 0.00 | 0.00 | 0.00 | 44.13 |
| S | 50.81 | 2.65 | 0.66 | 0.88 | 0.19 | 1.56 | 0.00 | 0.00 | 40.58 |
| A | 54.85 | 0.13 | 0.27 | 0.11 | 0.11 | 0.53 | 0.11 | 0.26 | 42.93 |
| D | 29.13 | 20.95 | 0.21 | 0.05 | 0.27 | 1.20 | 0.49 | 0.85 | 44.05 |

[a] LOC: Weight losses on calcination.

**Table 2. Crystal Size Distribution (vol %) of the Parent Carbonates**

| sorbent | <4 $\mu$m | 4−10 $\mu$m | 10−50 $\mu$m | >50 $\mu$m |
|---|---|---|---|---|
| B | 59.2 | 9.2 | 11.4 | 20.2 |
| H | 0.2 | 60.2 | 28.6 | 11.0 |
| C | 63.9 | 7.7 | 8.5 | 19.9 |
| P | 14.3 | 25.7 | 20.7 | 39.3 |
| K | 60.0 | 9.5 | 14.5 | 16.0 |
| M | 0.0 | 0.0 | 0.0 | 100.0 |
| S | 100.0 | 0.0 | 0.0 | 0.0 |
| A | 0.0 | 0.0 | 0.0 | 100.0 |
| D | 23.0 | 24.5 | 23.0 | 29.5 |

industries, and so forth. Nine different natural carbonates were fully characterized and subjected to repeated calcination/recarbonation cycles. The decays in sorbent activity with cycling, as well as their thermal and mechanical strength, were related to the characteristics of the parent carbonates and the textural development of the sorbents during cycling, and guidelines were obtained for the selection of the appropriate raw materials for the process investigated in this work.

## Experimental Section

Nine naturally occurring carbonates were selected for this study: five limestones, a dolomite, an ornamental marble, an aragonite, and a particulate mixture of shells from different crustaceans. The choice was not based on economy or availability but rather dictated by the decision to employ carbonates that represented the wide range that occur in nature in terms of chemical composition, crystal type, and crystal size distribution. These materials were ground and sieved to a diameter of 0.4−0.6 mm, the particle size used in the cycling experiments and also throughout the characterization work. The chemical composition of these samples was determined by atomic absorption (SRS 3000 Siemens) for the minor components and by classical redox volumetry techniques for the calcium. Crystallinities were estimated using X-ray diffraction (XRD; D5000 Siemens). Fourier transform infrared (FTIR) spectra were recorded on KBr pellets (sample/KBr = 1:400) using a Nicolet Magna 560 FTIR spectrometer with a spectral resolution of 4 $cm^{-1}$ in the 400−4000 $cm^{-1}$ range. Four pellets were prepared from each sample, in order to minimize experimental errors, and the spectra obtained were averaged after normalization. Bands due to symmetric stretch ($\nu_1$), asymmetric stretch ($\nu_3$), out-of-plane bend ($\nu_2$), and in-plane bend ($\nu_4$) were identified in the 400−2000 $cm^{-1}$ region of the spectra. Petrographic analyses of the samples were carried out at 500× magnification on thin sections of resin-embedded particulate blocks, using a transmitted light optical microscope with crossed polars. Various thin sections were prepared from each sample, and crystal sizes were estimated on 250 randomly selected points, using a mechanical point counter attached to the microscope stage.

The calcination/carbonation cycles were carried out in the small fixed-bed reactor apparatus schematized in Figure 1. It consists of a 1-m-high vertical furnace with two independent heating elements surrounding an alumina tube where a basket containing the sample is suspended along its vertical axis. A thermocouple is placed in the center of the particulate bed in order that the temperature of the sample can be monitored continuously. The reacting gases are axially injected at the base of the tube and are forced to pass through the basket and leave the furnace via the upper end of the tube. In our experiments, solids were allowed to react for 10 min for calcination (960 °C, 100% $CO_2$, middle position in the reactor) and 5 min for carbonation (650 °C, 100% $CO_2$, top of reactor). The basket was automatically raised and lowered by means of an engine placed above the furnace. Selected subsamples were rapidly withdrawn from the basket when it was in its upper position, using a suction probe, and their activity was determined by sample weight loss at 900 °C in a thermogravimetric apparatus (Setaram TAG24).

The decrepitation resulting from the thermal shock undergone by the sorbents was evaluated by sieving size-graded samples (0.4−0.6 mm) after a single calcination/carbonation cycle and weighing the newly formed size fractions <0.1, 0.1−0.2, 0.2−0.3, and 0.3−0.4 mm. Similarly, the mechanical strength of the sorbents was estimated by sieving the samples after one calcination/carbonation cycle and a mechanical resistance test. The device for this test consisted of a spinning cylinder ($L$ = 32 cm, Ø = 3 cm, 25 rpm, 4 min) loaded with 2 g of samples and six steel balls. These conditions were not intended to simulate those prevailing in a fluidized bed, but they can be used to arrange the sorbents tested according to their mechanical resistance during cycling.

Finally, the evolution of the pore network of the sorbents during cycling, in both their calcined and recarbonated forms, was studied by mercury porosimetry (Micromeritics 9500).

## Results and Discussion

**1. Description of Samples.** *1.1. Chemical Composition and Crystallinity.* The results from the chemical characterization of the samples are given in Table 1, and the crystal size distribution data obtained by point-counting analysis are shown in Table 2. Figure 2 plots the XRD and FTIR spectra of the samples. With these data, plus the a priori information on which the selection was based, the samples can be described as follows: La Blanca (B) is a Spanish high-purity limestone, and Havelock (H) and Cadomin (C) are Canadian commercial fine-grained limestones of medium purity. A marble (M) was selected because of its high purity and crystallinity. It exhibits the same trigonal crystal structure as calcite. Planadera limestone (P) was included as it is representative of bioclastic limestones where the calcite crystals are parts of biogenic structures, and therefore the fabric of the rock is controlled by the accumulation of fossil debris. Piasek limestone (K) was previously reported as a carbonate showing good cycling properties. To study the influence of the crystal type on the calcinations/recarbonation process, a sample consisting of crustacean shells (S) was also selected, as these materials are typically rich in amorphous calcium carbonate.[23] Aragonite (A) is the orthorhombic polymorph of calcium carbonate. The Sierra de Arcos dolomite (D) was included in order to widen the range of carbonate compositions. Both the

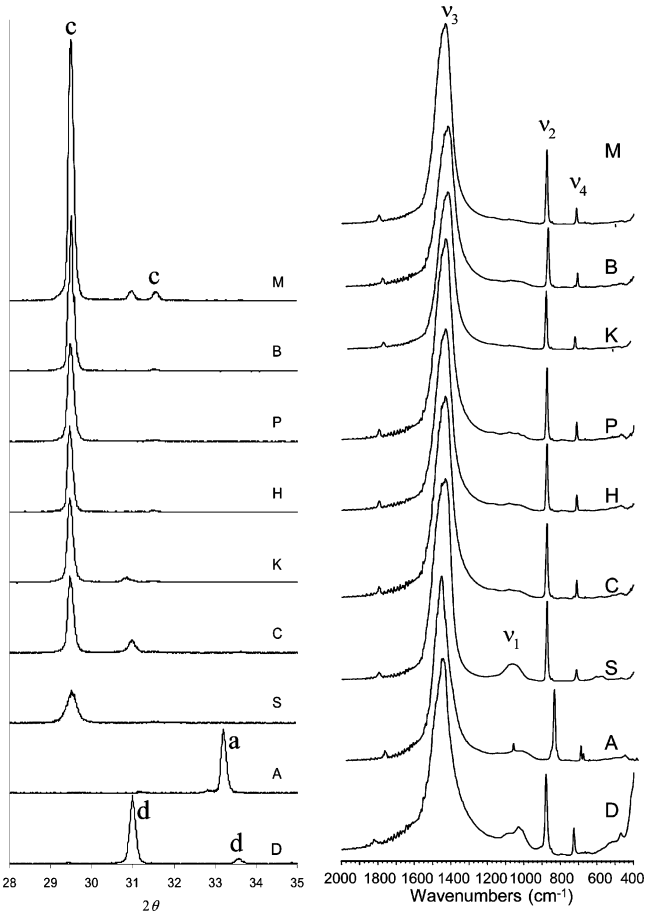


**Figure 2.** Left: XRD diffractograms of the sorbents (c: calcite; d: dolomite; a: aragonite). Right: FTIR spectra of the sorbents ($\nu_1$: symmetric stretch; $\nu_2$: out-of-plane bend; $\nu_3$ asymmetric stretch; $\nu_4$: in-plane bend).

XRD and IR spectra (Figure 2) indicate only small impurities in the selected samples. The XRD spectra of P, H, and S only display the peaks attributable to calcite, whereas the M and C spectra also have low-intensity peaks that are assigned to dolomite. The intensity of the main calcite peak at $2\theta = 29.5°$ in the XRD spectra followed the sequence M > P ∼ H > C > S, indicating a decrease in crystallinity. D and A consist of quite pure dolomite and aragonite, respectively. The IR spectra of the carbonates are dominated by the band attributed to asymmetric stretching ($\nu_3$) at 1434 $cm^{-1}$ for calcite (M, P, H, C, and S), at 1439 $cm^{-1}$ for dolomite (D), and at 1477 $cm^{-1}$ for aragonite (A). The bands due to out-of-plane bending ($\nu_2$) and in-plane bending ($\nu_4$) appear at 877 and 715 $cm^{-1}$ in the IR spectra of the calcium carbonates which show calcite structure, respectively, as can be seen in Figure 2. The symmetric stretching band ($\nu_1$) at 1064 $cm^{-1}$ is strictly forbidden in the IR spectra of a calcite crystal, and its presence is commonly attributed to the occurrence of poorly crystallized material. A broad band centered at 1068 $cm^{-1}$ was observed in the spectrum of the crustacean shells (S) whose presence is reported as being the most characteristic feature of the IR spectra of amorphous calcium carbonate.[23] The position of the $\nu_2$ band at 860 $cm^{-1}$and the $\nu_4$ double band at 713 and 701 $cm^{-1}$ in the aragonite spectrum confirms the orthorhombic structure of the crystals but also appears to indicate a certain substitution of Sr for Ca,

(23) Addadi, L.; Raz, S.; Weiner, S. Taking Advantage of Disorder: Amorphous Calcium Carbonate and its Roles in Biomineralization. *Adv. Mater.* **2003**, *15*, 959−970.

**Table 3. Particle Size Distributions (wt %) after One Calcination/ Recarbonation Cycle**

| sorbent | <0.1 mm | 0.1−0.2 mm | 0.2−0.3 mm | 0.3−0.4 mm | 0.4−0.6 mm |
|---|---|---|---|---|---|
| B | 0.0 | 0.0 | 0.5 | 5.2 | 94.3 |
| H | n.a. | n.a. | n.a. | n.a. | n.a. |
| C | 0.0 | 0.0 | 0.0 | 0.0 | 100.0 |
| P | 1.0 | 1.5 | 1.0 | 3.9 | 92.7 |
| K | 0.0 | 0.0 | 0.0 | 0.0 | 100.0 |
| M | 1.4 | 17.6 | 36.2 | 23.8 | 21.0 |
| S | 0.9 | 0.5 | 0.5 | 15.3 | 82.9 |
| A | 1.4 | 1.4 | 4.7 | 6.6 | 85.8 |
| D | 0.0 | 0.0 | 0.0 | 0.0 | 100.0 |

**Table 4. Particle Size Distributions (wt %) after One Calcination/ Recarbonation Cycle and a Mechanical Test**

| sorbent | <0.1 mm | 0.1−0.2 mm | 0.2−0.3 mm | 0.3−0.4 mm | 0.4−0.6 mm |
|---|---|---|---|---|---|
| B | 5.7 | 6.4 | 7.9 | 15.1 | 64.8 |
| H | n.a. | n.a. | n.a. | n.a. | n.a. |
| C | 5.6 | 6.6 | 9.4 | 13.1 | 65.2 |
| P | 9.4 | 8.2 | 11.1 | 15.2 | 56.1 |
| K | 3.9 | 5.9 | 8.8 | 12.0 | 69.3 |
| M | 14.5 | 36.8 | 33.8 | 11.8 | 3.2 |
| S | 27.6 | 11.5 | 15.7 | 20.3 | 24.9 |
| A | 17.1 | 18.5 | 20.4 | 18.5 | 25.6 |
| D | 17.1 | 12.5 | 15.1 | 16.1 | 39.2 |

which is quite common in aragonite crystals. Characteristic dolomite bands at 881 $cm^{-1}$ ($\nu_2$) and at 732 $cm^{-1}$ ($\nu_4$) were observed in the IR spectrum of the dolostone (D), but the shift to higher frequencies of the $\nu_3$ band (1452 $cm^{-1}$), closer to the position expected for ankerite, could indicate some substitution of Fe for Mg in the dolomite structure. The presence of dolomite in the spectrum of C is confirmed by the weak band at 729 $cm^{-1}$.

Two aspects were taken into account when the thin sections of the carbonate pellets were examined through the microscope: the size of the crystal under the crosswire, regardless of the accompanying crystals in the particle (Table 2), and the heterogeneity of the particle in terms of crystal size. Everything considered, the appearance of the particles in the carbonates studied was rather different. The microphotographs of Figure 3 show typical examples of particles that display the different grain size classes presented in Table 2.

The marble particles were mainly polycrystalline with single crystals exceeding 50 $\mu$m. H can be defined as a microsparitic limestone where most of the particles consist of sparry crystals (4−10 $\mu$m) with disseminated crystals of larger size. C mostly consists of rather heterogeneous grains with a micritic texture (crystals smaller than 4 $\mu$m) that surround dispersed crystals of larger size. These dispersed crystals are often rhombohedric in shape, which indicates a late replacement of dolomite crystals. P is a bioclastic limestone with abundant crinoid remains and a wide distribution of crystal sizes (Table 2). The crustacean shells consist of amorphous calcium carbonate, which is seen under the optical microscope as an isotropic material, plus some calcite crystals that retain the original structure of this biological material. A wide distribution of crystal sizes is also observed in the dolomite, although in this case the texture of the individual particles is rather homogeneous. The aragonite particles consist of single monocrystal particles.

The crystal sizes reported in Table 2 for the carbonates with a calcite structure match well with the intensities of the main calcite peak in the XRD spectra of Figure 2:

$$\text{Crystal size: } M \gg P > H > B > K > C \gg S$$

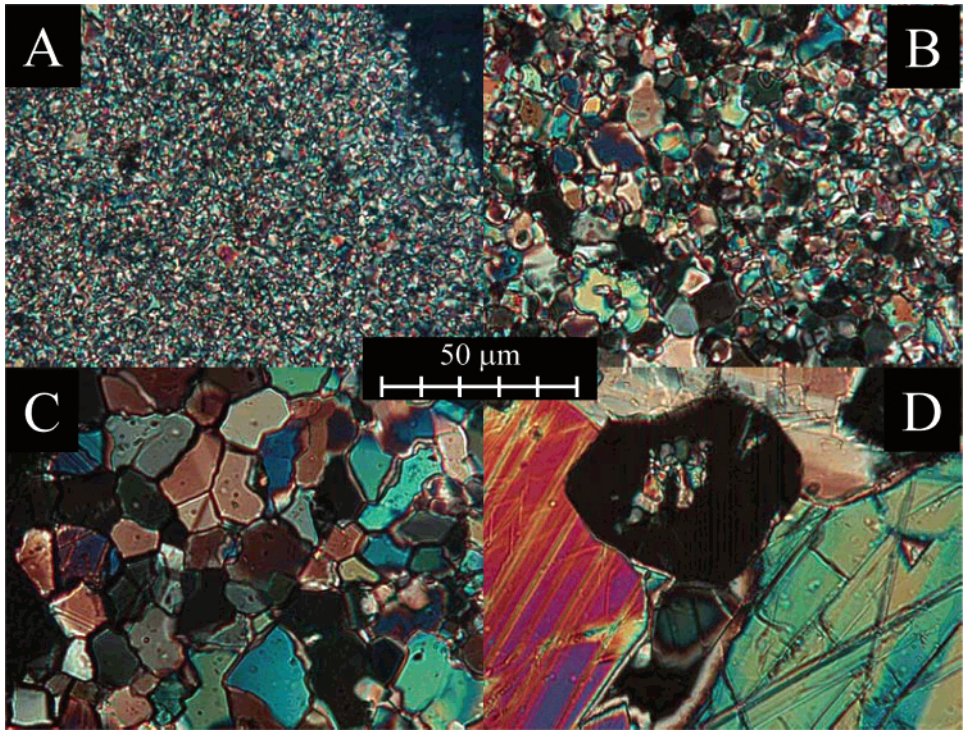


**Figure 3.** Micrographs showing the different crystal size classes used in the petrographic characterization of the samples. A: Micritic texture (<4 $\mu$m); B: sparry (4−10 $\mu$m); C: 10−50 $\mu$m; D: >50 $\mu$m. Transmitted polarized light.

*1.2. Resistance to Thermal and Mechanical Shock.* Tables 3

Intensity of the calcite peak (XRD): M ≫ B ≫ P > H = K > C ≫ S

and 4 show the particle size distributions of the sorbents after one pass through the calcium loop, with and without further mechanical testing. According to these data, the studied sorbents can be arranged in terms of their increasing thermomechanical resistance as follows:

Resistance to decrepitation: D ≈ K ≈ C > B ≈ P > A ≈ S > M

These tests were not applied to H limestone due to problems of

Resistance to decrepitation + mechanical shock: K ≈ C ≈ B > P > D > A ≈ S > M

sample availability, but the observed behavior of this limestone when it was introduced in the furnace for the cycling experiments (crackling) suggests that its tendency to decrepitation must be quite low, that is, comparable to that of limestone K.

**2. Behavior of Samples in the Calcination/Carbonation Loop.** *2.1. Sorbent Efficiency.* The conversion decay curves during the cycling of the studied carbonates are given in Figure 4, where a continuous decay in the activity of all the sorbents with the number of cycles can be observed. The decays are greater in the first 10−30 cycles and then become less pronounced up to ~60 cycles, where a quite low residual activity value is reached and roughly maintained throughout the rest of the cycles. Within this general trend, some differences can be observed between the sorbents studied. Thus, the carbonation conversion in the first cycle ranged from 65% for the marble (M) and limestone B to 32% for the aragonite (A) and the carbonate shells (S). On the other hand, the residual conversions

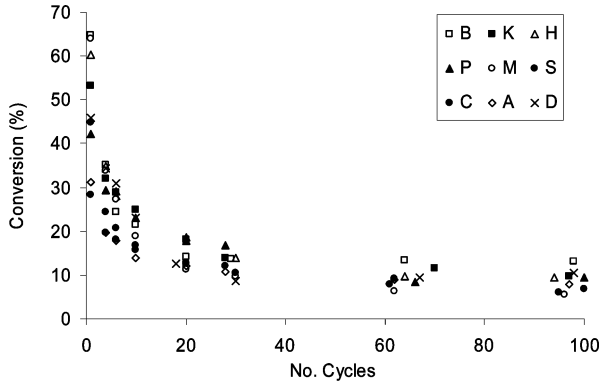


**Figure 4.** Variation of sorbent performance during cycling.

after 100 cycles ranged from the 13% achieved by limestone B to a poor 6% for limestone C and the marble.

It should be pointed out that these conversions were calculated as the fraction of the CaO contained in the samples which was converted into $CaCO_3$. This was done in order to compare the intrinsic activities of the CaO in their various crystalline and chemical occurrences. However, from a practical point of view, it is more realistic to consider the amount of $CO_2$ captured per gram of calcined sorbent, as this tells us straightaway the quantities of material required to achieve a given $CO_2$ retention. This is shown in Figure 5, where the cumulative plots of captured $CO_2$ per gram of sorbent in the loop versus the number of cycles can be used to compare the performances of the sorbents during the cycling experiments. The choice of an optimum calcareous sorbent will depend on the characteristics of the calcium looping system. Thus, if a relatively large amount of sorbent is to be purged from the system and replaced by fresh limestone, then the sorbent particles will be statistically cycled only a limited number of times, and the performance of the capture system will be better, the higher the initial activity of the sorbent and the slower the decay of this activity. However,

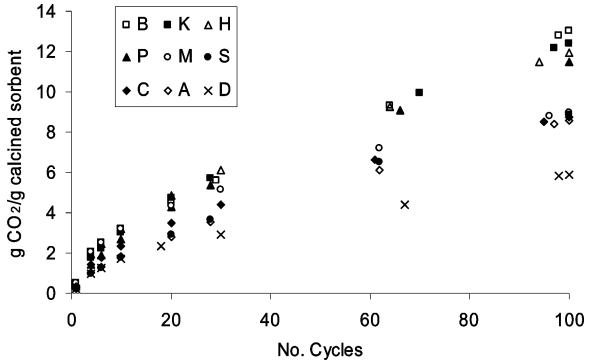


**Figure 5.** Cumulative $CO_2$ capture of the sorbents during cycling.

if the system is intended for the prolonged use of the sorbent, then the residual activity after a long number of cycles will acquire more importance. For the sorbents studied here, and on the basis of the amount of $CO_2$ captured per gram of sorbent after 30 and 100 cycles, the raw materials could be arranged as follows:

Performance after 30 cycles: $D \approx A \approx S < C < M \approx P \approx B \approx K \approx H$

All the limestones except Cadomin (C) displayed the highest

Performance after 100 cycles: $D < A \approx C \approx M \approx S \ll H \approx P \approx K \approx B$

$CO_2$ retention capacities under both the low and the high residence time scenarios. The dolomite, despite the comparatively high performance of its CaO (see Figure 4), was the worst of all the sorbents due to its inherently high loading of inert components (MgO). The marble (M) and the caparace sample (S) are opposed to each other in various respects: M is a highly pure and crystalline carbonate, whereas S has the lowest $CaCO_3$ contents (excluding the dolomite, see Table 1), and it is by far the least crystalline of all the sorbents tested. The deactivation curves given in Figure 4 show that the performances of these two sorbents are accordingly very different, M showing the highest initial reactivity and S displaying the lowest. On the other hand, the residual activity was quite low for both samples. Finally, the aragonite (A) sample displayed the lowest initial reactivity, together with sample S, and its residual activity was also rather low compared with the rest of the sorbents tested.

*2.2. Evolution of the Pore Network.* Figure 6 illustrates the typical appearance of the pore size distribution of a calcined limestone—a large population of small-sized pores and a smaller volume made up of voids of larger size, probably cracks generated during calcination. The pore network of the sorbents can thus be reasonably described by the pore diameter at which the distributions peak. The specific pore volume for this calcined sorbent is 0.35 mL $g^{-1}$, close to the theoretical value of 0.36 mL $g^{-1}$, although other sorbents and/or numbers of cycles may eventually yield lower pore volumes as a consequence of particle shrinkage.

Figure 7 shows the variation of the peak pore diameters with the number of calcination/carbonation cycles. Sample S was not included in this figure because its pore diameters were too large (3000−15 000 nm) to allow the graph to be properly scaled. These enlarged pore diameters probably reflect the ornament of the material, which already existed in the raw sample. The rest of the samples display widely varying behaviors, from the almost invariant pore sizes of the marble to the large and continuous increase observed in limestone C.

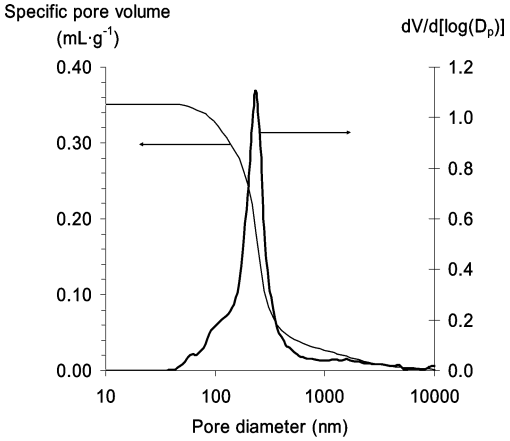


**Figure 6.** Pore size distribution of a limestone (C) calcined at 960 °C under $CO_2$.

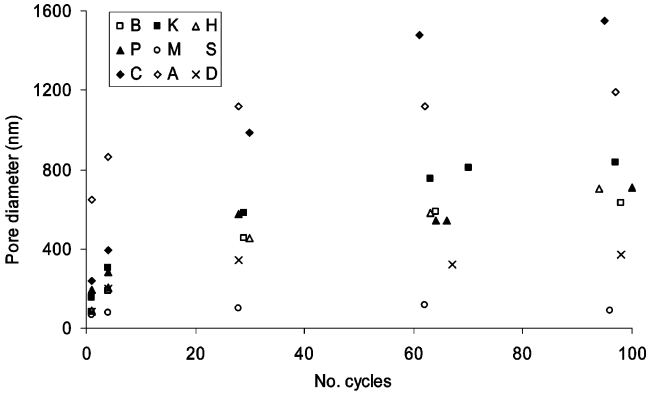


**Figure 7.** Evolution of peak pore diameters of the calcines during cycling.

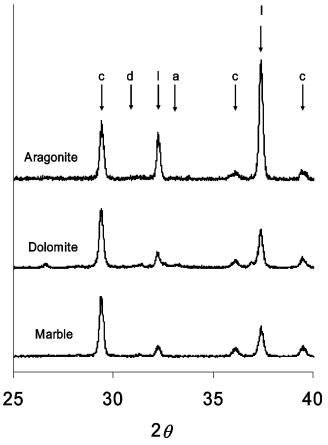


**Figure 8.** XRD diffractograms of sorbents subjected to one calcination/carbonation cycle (c: calcite; d: dolomite; l: lime; a: aragonite).

It is particularly remarkable that the aragonite (A) generated very large pores even in the first calcination stage (650 nm), which then increased at moderate rates during cycling. Moreover, this sample shares with the marble a very high crystallinity (100% >50 mm crystals, see Table 2) and a quite high purity (Table 1), but the mean pore size of the calcined marble was 10 times smaller than that of the aragonite. Unless the slightly higher strontium content of the A sample is taken into account, the unusual pore size distribution of the calcined aragonite has to be attributed to its orthorhombic crystal arrangement, as opposed to the triclinic polymorph present in the rest of the samples. This influence of the crystal type on the calcination behavior of the aragonite is illustrated in Figure 8, which plots

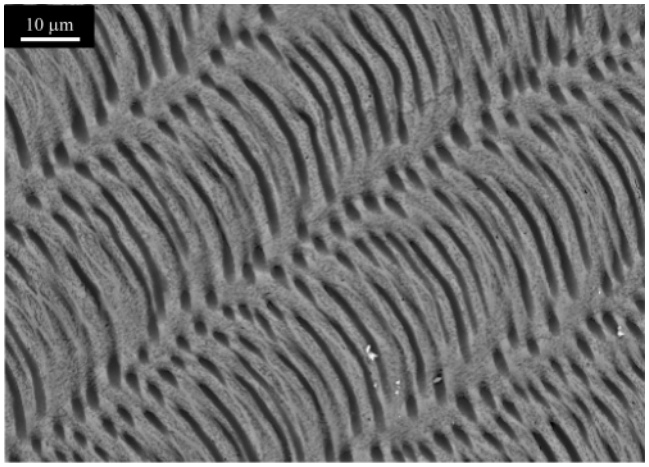


**Figure 9.** SEM image showing the highly textured arrangement of the parent S sample.

the XRD diffractograms of an aragonite, a marble, and a dolomite sample, all three of which were subjected to a single calcination/carbonation cycle. In this figure, it can be seen that the peaks at $2\theta = 32.3$ and 33.4° and assigned to CaO are much more intense in the aragonite sample than in the marble sorbent, even if the higher percentage of lime in the aragonite-derived sorbent is taken into account. It seems therefore that the initial arrangement of the atoms in the aragonite sample promotes the formation of a more crystalline lime on calcination. Of course, the cycling of the dolomite does not bring it back to its former crystal arrangement because the temperature of carbonation is too high to allow the formation of a Mg carbonate. Bearing in mind the peculiar behavior of the S and A samples, the sorbents can be arranged according to their tendency to sinter, which was estimated by the mean pore sizes of their calcines after 100 cycles, as follows:

$$M \ll D \ll B \approx P \approx H < K\ (\ll A) \ll C\ (\ll S)$$

**3. Discussion of Results.** The characteristics of the pore network of the CaO, generated during the calcination of a calcareous sorbent as a consequence of the different molar volumes of calcium oxide and carbonate, will have a strong influence on the conversion achieved in the subsequent carbonation stage of the calcium loop. The pores in the calcined particles will host the extra solid volume generated on recarbonation, and as the newly formed carbonate will form a product layer on the pore surfaces of the CaO, high $CO_2$ capture capacities will be obtained from sorbents with high surface areas and pore sizes large enough to accommodate a thick product layer. These two conditions cannot be satisfied simultaneously, since, for materials with very similar specific pore volumes, the larger the surface area, the smaller the pore size. There is, however, one more physical limitation to the reaction between the CaO and the $CO_2$, that is, the increasing difficulty the $CO_2$ has in permeating the carbonate layer and reaching the unreacted CaO core. As a consequence, after reaching a certain thickness, the carbonate layer progresses too slowly for purposes of $CO_2$ capture.

In a recent paper,[24] it was reported that the maximum thickness of this product layer is 50 nm, after which the reaction becomes diffusion-controlled. This translates into a reduction of pore diameter of around 25 nm (the rest is the space formerly occupied by the reacted CaO), so that the pore network of the CaO should ideally be formed by pores of around 50 nm in diameter.

Bearing this in mind, as all the calcines studied here had larger pores (see Figure 7) than the threshold size where diffusional hindrances start, the capture capacity of the sorbents should be higher, the lower the size of the pores. Rearranging the calcined sorbents according to their increasing capture efficiency and decreasing pore size leads to the following:

$$\text{Decreasing pore diameter (100 cycles):}\ (S) \gg C\ (\gg A) \gg K > H = P = B \gg D \gg M$$

The major discrepancies are found for the dolomite (D), the

$$\text{Increasing performance (100 cycles):}\ D < A \approx C \approx M \approx S \ll H \approx P \approx K \approx B$$

marble (M), and the mixture of caparaces (S). Dolomite is known to have a much lower tendency to sinter than limestone, which explains the comparatively small size of its pores. On the other hand, the low capture capacity of this sorbent is due to its inherently high percentage of inerts (MgO). As regards the biogenic sample (S), it has already been mentioned that the pore size distribution of its calcine is dominated by the fabric of the original structures of the crustacean shells. Figure 9 is a scanning electron microscope (SEM) image that shows the rich ornamentation in this sample, suggesting that the capture capacity of this sorbent must at least in part be conditioned by the surface area of the parent carbonate.

The case of marble deserves a detailed analysis, as this sample is composed exclusively of monocrystal particles, which can also be found in polycrystalline limestones (see Table 2). On calcination, the marble generated the narrowest porous network of all the sorbents tested (65 nm peak diameter) and maintained it over 100 calcination/carbonation cycles. However, this only gave rise to a high capture capacity in the first few cycles. This capacity decreased rapidly to a point where the sorbent displayed the lowest efficiency of all the carbonates. A similar combination of low conversion and small-sized pores has been reported[20] and was attributed to the formation of a sealing carbonate layer on the surface of the former crystals which made up the sorbent. In this case, the sorbent under study was the same B limestone as that used in this work, and the sealing of the pores was caused by the longer carbonation times used (30 min). A study of these samples led to the conclusion that the pore sizes detected by mercury porosimetry did not correspond to the actual pore sizes in the samples but rather to the existence of bottlenecks at the entrances of the pore network of the particles. The practical implications of this pore morphology are a reduced surface area, compared to the value expected from the pore size distribution and porosity, and a tendency for the pores to close during carbonation. In the paper just mentioned,[20] a method was proposed to estimate the volume of closed pores in a recarbonated sample, which consisted in calculating the true density of the sample from the contributions of the carbonate formed ($\rho = 2.70$ g cm$^{-3}$) and the unreacted lime ($\rho = 3.40$ g cm$^{-3}$) and then comparing the value thus obtained with the density obtained by porosimetry at maximum Hg penetration (pores > 5.5 nm). The discrepancy between the two density values thus obtained is related to the occluded pore volume through

$$V_o = \frac{1}{\rho_{\text{experimental}}} - \frac{1}{\rho_{\text{theoretical}}}$$

The same methodology was applied to the sorbents studied here

(24) Alvarez, D.; Abanades, J. C. Determination of the critical product layer thickness in the reaction of CaO with $CO_2$. *Ind. Eng. Chem. Res.* **2005**, *44*, 5608−5615.

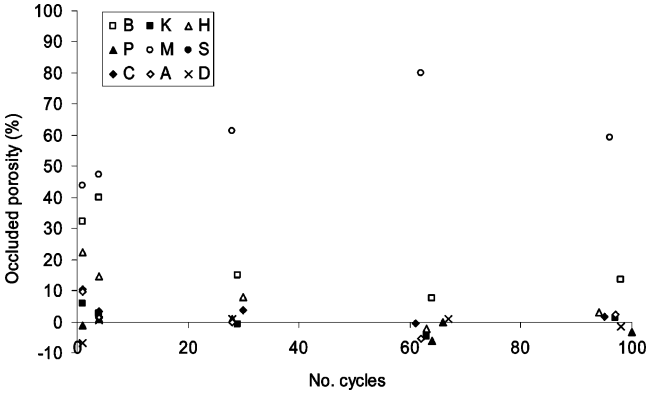


**Figure 10.** Percentage of closed-pore volume in the recarbonated sorbents.

with the result shown in Figure 10, which plots the variation of the occluded pore volume, expressed as a percentage of the total pore volume (opened + closed) in the recarbonated samples during cycling. In this figure, it can be readily seen that most of the samples only had appreciable closed volumes in the first few cycles, where the carbonation is more extensive and the pores are still only slightly sintered. A notable exception to this is the behavior of the marble, whose percentage of closed porosity amounts to over 40% even at high levels of cycling. This is clear proof that the $CO_2$ cannot take full advantage of the pore network. It is also unlikely that a pore network with a uniform diameter of around 70 nm (no bottlenecks) will only reach the low conversions displayed by this sorbent and, at the same time, undergo extensive sealing. Of course, we recognize that the calculations used to obtain the percentages of closed pore volume are subject to experimental errors, as evidenced by some negative (although of small magnitude) values plotted in Figure 10. However, the differences between M and the rest of the samples are big enough to confirm the above-mentioned sealing effect. In order to illustrate this, a few particles from a recarbonated sorbent, obtained after cycling the marble 100 times, were mildly crushed by pressing them between two pieces of glass, and these particles were then gold-coated and placed onto the stage of the SEM for the examination of their outer and fracture surfaces. The outer surface of this sample has the appearance shown in Figure 11a, with far fewer and smaller pores than on the fracture surface of Figure 11b. Figure 11b also shows that the fracture surface perpendicular to the sheet plane and attributable to decrepitation in an early stage of cycling presents basically the same features as the outer surface of those in Figure 11a. In any case, the size of the pores shown in Figure 11b, about 1 $\mu$m, is far larger than the 70 nm diameter reported by the mercury porosimetry technique, and the surface area of these pores should be accordingly much smaller and unable to react extensively with the $CO_2$, as shown in Figure 4.

If we consider just the limestone-based sorbents, Cadomin limestone (C) showed the lowest capture capacity (Figures 4−5). The reason for this is the pronounced tendency of this sorbent to sinter, resulting in calcines with pore radii 2−3 times larger than those of the other limestone-derived sorbents. The characterization data for this limestone, given in Tables 1 and 2, do not show major differences with the rest of the limestones, except for its somewhat higher Mg content. The doping of calcite with moderate amounts of Mg might enhance the ionic mobility in the crystal lattice, thus favoring the sintering of the calcine. In fact, the Mg contents of the limestones match well with the pore diameters of the corresponding highly cycled calcines. Of course, the exceptionally high Mg loading of the dolomite is a drawback rather than an advantage for the ionic mobility of its calcine.

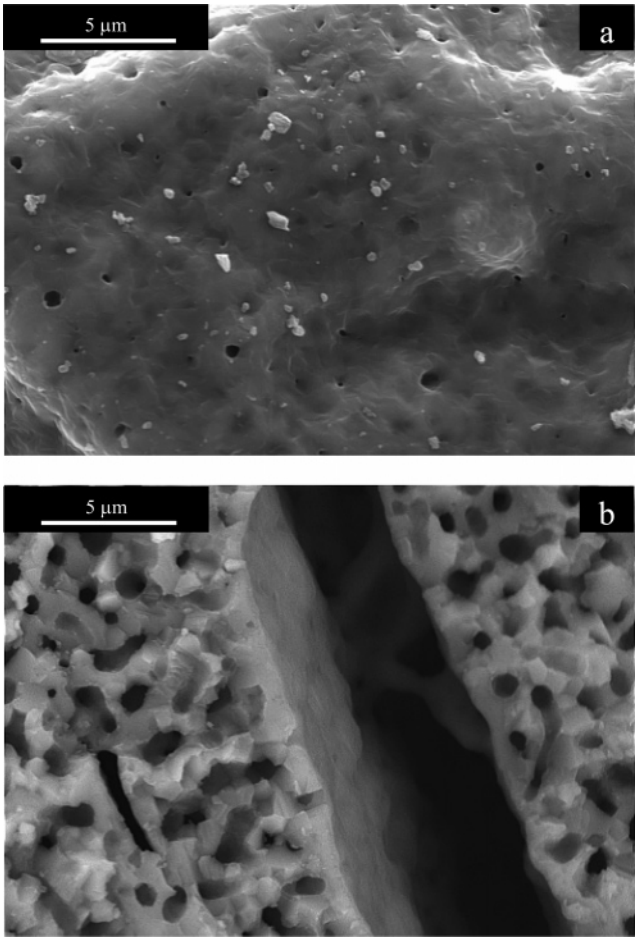


**Figure 11.** (a) Outer surface of a sorbent particle (M, 100 cycles, recarbonated). (b) Fracture surface of the same sorbent, showing its internal pore network and a decrepitation crack (perpendicular to the sheet plane).

Finally, the tests carried out to evaluate the thermal and mechanical resistance of the sorbents confirmed that the larger the crystallite size, the lower the resistance to decrepitation and abrasion. The highly crystalline samples M and A were highly degraded by both thermal and mechanical shock. The limestones showed the best thermomechanical properties, and the dolomite displayed very good thermal stability but, despite the small size of its crystal grains, a low resistance to mechanical shock, probably due to its chemical composition, inherently different from that of the limestones. In fact, the somewhat lower resistance of P limestone, compared to the rest of the limestones studied, can be attributed to its higher proportion of large crystals (see Tables 2−4). The fragility of the S sample should not be attributed to its crystal structure but, again, to the thin-walled arrangement of this material (Figure 9).

## Conclusions

When searching for a suitable sorbent to be used in a calcination/carbonation loop, both its capture ability and resistance to thermal and mechanical shocking have to be taken into account. In the case of the limited set of sorbents studied here, it can be concluded that (1) limestones tend to behave better than aragonite, dolomite, highly crystalline carbonates, or amorphous carbonates; (2) dolomites have a good resistance to thermal shock, but very bad mechanical strength; (3) limestones

made up of small (<4 $\mu$m) crystals have better mechanical properties; (4) magnesian limestones show poorer capture abilities than pure calcium carbonates. Of the various sorbents tested, B and K limestones showed the best combination for good performance both in a short- and in a long-lasting loop and a high resistance to size degradation.

The samples studied in this work are not comprehensive of the wide variety of carbonates available, but the results found suggest that only a minor improvement of the cycle efficiency of this $CO_2$ capture system can be expected from the search for "exotic" naturally occurring sorbents. Other options such as the design of synthetic sorbents or the enhancement of the rate of sorbent utilization by reactivation could be a more practical approach if this promising technique is to become applicable on an industrial scale.

**Acknowledgment.** Financial support through the ULCOS Integrated Project (ref: 515960) is gratefully acknowledged. D.A. is grateful to C. P. Vega de Guceo for the kind donation of the crustacean shell sample.

EF060573I